Journal of Theoretical and Applied Information Technology
15st September 2026. Vol.104. No.17

ISSN: 1992-8645 www.jatit.org E-ISSN: 1817-3195

DEEP GRAPH ATTENTION NETWORKS FOR MRI BRAIN TUMOR CLASSIFICATION AND SPECTRAL ANALYSIS

RAJESWARI R[1] , SUJATHA N[2,*]

[1,2*] Department of Mathematics, SRM Institute of Science and Technology, Ramapuram Campus, Chennai 600089, India

E-mail: [1]rr3655@srmist.edu.in, [2,*]sujathan@srmist.edu.in

ABSTRACT

Classification of brain tumors based on MRI is essential in neuro-oncology. Conventional CNN algorithms treat images as structured grids and do not necessarily consider spatial interaction between image regions. In our paper, we develop a method that represents an MRI image through a graph structure, treating image regions as graph nodes associated with feature vectors and modeling interactions between regions through weighted edges. We experimentally compare GCNs with the proposed GAT model, which incorporates edge features into the attention mechanism. We evaluate their ability to classify three classes of tumors, namely glioma, meningioma, and pituitary tumors, achieving a classification accuracy of 77.37%, which surpasses the performance of GCN (71.53%) and conventional approaches (76.67%). Our spectral analysis of graph node features shows that different structures characterize each tumor type. Moreover, the proposed attention mechanism allows us to visualize diagnostically valuable areas of the image.

Keywords: *MRI, Brain Tumor Classification, Graph Neural Networks, Graph Attention Networks, Spectral Graph Properties*

1. INTRODUCTION

Brain tumors represent one of the most important classes of neurodegenerative disorders from simple benign tumors to more complex malignant tumors. It is important to have proper and timely classification of brain tumors to help in treatment and improving patient outcomes. Magnetic Resonance Imaging (MRI) is considered an important tool to diagnose brain tumors thanks to its superiority in image contrast as well as being non-invasive. However, there is still a lot of difficulty in manual classification, which raises the importance of computer-assisted diagnosis using AI.

Deep Learning, particularly Convolutional Neural Networks (CNN), has proven quite successful in medical images classification. Although CNN models can be effective in capturing local features, they lack the ability to learn spatial relations between pixels as well as the complexity associated with brain tumors. Additionally, brain tumor classification comes with various challenges, including heterogeneous nature, data scarcity, imbalance between the different classes, and analyzing multiple MRI images at once.

One of the possible ways to overcome the stated problems may be the usage of graph-based learning algorithms. In this case, each node corresponds to an image region, and the edges correspond to the connection between the nodes. Graph neural networks (GNN), including GCN and GAT algorithms, have been proven to be capable of learning structures and contexts from the graph representation. As a result, this kind of algorithms is capable of capturing long-range dependencies and interactions between tumor regions and adjacent tissue regions. It will help improve classification performance and provide insights into the learned model. In this research paper, we propose a new way of classifying brain tumors from MRI images using the graph-based algorithm. We propose improving the Graph Attention Network model by introducing edge features to enhance the classification performance.

2. RELATED WORK

2.1 Traditional Approaches To Brain Tumor Classification

Early brain tumor classification approaches using automation mainly consisted of feature extraction from MRI images, which were then used with traditional machine learning techniques. Normally, the features included morphological, textural, and statistical characteristics [17].

Combining the use of texture information extracted using GLCM texture features together with SVM, Kharrat et al. [18] were able to achieve 91.23% accuracy for the classification task involving three classes. Similarly, Zacharaki et al. [19] applied SVM to classify tumors by first extracting features from multi-parametric MRI images using intensity, shape, and texture information and achieving 85% accuracy in distinguishing between metastases and gliomas.

Despite the promising results shown by such approaches, their success relied heavily on the designed feature extraction techniques, which required specific knowledge and may not be effective in capturing the intricate structures of brain tumors [20].

2.2 Deep Learning For Brain Tumor Classification

The field of deep learning has seen many breakthroughs when it comes to the analysis of medical images through automatic feature detection. CNNs have widely been used for the classification of brain tumors due to their ability to extract hierarchical features. Afshar et al. [21] proposed a method called CapsNet, which was successful in achieving an accuracy rate of 90.89%, while on the other hand, Swati et al. [22] employed transfer learning using the VGG19 model and achieved 94.82% accuracy. Using CNN for multi-grade tumor classification along with data augmentation gave Sajjad et al. [23] an accuracy rate of 90.67%. However, CNN models assume image inputs as regular grids and hence are inappropriate for brain tumors.

2.3 Graph-Based Approaches In Medical Imaging

Graph-based methods have become quite popular recently in the field of medical imaging due to their ability to represent the irregular structure of the object and complicated relationships in space. There have been many studies involving the use of graph-based methods in medical imaging applications including the identification of brain tumors. For example, Li et al. [25] proposed a spectral clustering approach based on graph theory for the segmentation of brain tumors.

The method proposed by Parisot et al. [26] employed graph theory to provide semi-supervised learning based on spatial and similarity characteristics. For classification tasks, a model of GNN was developed by Kazi et al. [27] for chest X-ray image analysis. Zhang et al. [28] applied GCNs for examining the interaction between cells in histopathology images. To date, there have been limited studies using graph theory, particularly GAT, to classify brain tumors via MRI scans.

2.4 Attention Mechanisms In Neural Networks

Attention mechanisms have been introduced into deep learning models, becoming a vital component since they enable the model to concentrate on particular features of the input data. Although attention mechanisms were originally applied to tasks related to natural language processing, they gained rapid popularity among other domains such as medical image analysis. According to Schlemper et al. [30] and Oktay et al. [31], attention-based neural networks showed good performance in the context of pancreas segmentation and cardiac MRI analysis, respectively. The concept of weighting nearby nodes differently could be transferred to graph neural networks. Specifically, Veličković et al. [16] proposed the idea of creating Graph Attention Networks (GATs). Despite their success in different fields, there is a lack of research on GATs' potential for analyzing MRI images in brain tumor classification.

2.5 Spectral Graph Theory In Image Analysis

Spectral graph theory focuses on examining the graph based on the eigenvalues and eigenvectors of the matrix associated with it, including Laplacian and adjacency matrices, to discover certain features [32]. Spectral graph theory and related techniques are often utilized in image processing for image segmentation [33], clustering [34], and even dimensional reduction [35]. Zhang and Hancock [36] used spectral graph theory in the context of texture analysis, while Shiee et al. [37] used spectral clustering for brain MRI segmentation. But still, few studies focus on exploring how spectral graph features can be employed for brain tumor characterization and classification by GNNs.

3. MATERIALS AND METHODS

3.1 Dataset Description and Preprocessing

Three types of brain tumors glioma, meningioma, and pituitary tumors were present in a publicly available dataset of brain MRI scans used in this work. MRI images with T1-weighted contrast-enhancement gathered from several medical centers made up the dataset. There were 4,526 training images and 411 validation images in all, with a

distribution like this: **Glioma**: 1,153 training images, 136 validation images; **Meningioma:** 1,449 training images, 140 validation images; **Pituitary:** 1,424 training images, 136 validation images. Each image was accompanied by a label file indicating the tumor type and bounding box coordinates (in the format: class_id, x_center, y_center, width, height).

Figure 1: MRI Preprocessing Pipeline for Graph Construction

The figure 1 showing the essential steps involved in the pre-processing phase of magnetic resonance imaging (MRI) scan data to identify tumors, such as normalizing intensities, identifying the tumor ROI, and validating the dataset.

3.2 Graph-based Representation of MRI Images

3.2.1 Graph Construction

We represent each MRI image as a graph $G = (V, E)$, where $V = \{v_1, v_2, v_3, \dots, v_n\}$ represents the set of nodes and $E \subseteq V \times V$ denotes the set of edges. Node v_i depicts a portion of the picture, while edge $e_{ij} = (v_i, v_j) \in E$ denotes the association among regions. Graph building includes the following phases:

A. Grid Partioning: The MR image is partitioned into a grid of 16 × 16, leading to 256 cells of equal sizes.

B. Node Creations: Every cell is turned into a node of the graph, where the feature vector xi is computed for each image block.

C. Edge Creation: Edges are formed between the adjacent cells of nodes (8 connected).

3.2.2 Node Feature Extraction

For each image region to be modeled as a graph node, we define the feature vector $x_i \in \mathbb{R}^d$ that encodes visual and geometric information. The basic feature set comprises five elements: normalized mean RGB intensities, gradient magnitude, and spatial identity. Specifically, the feature vector is defined as

$$x_i = \left[\frac{R_i}{255}, \frac{G_i}{255}, \frac{B_i}{255}, \frac{\nabla_i}{255}, \mathbb{I}(v_i \in ROI)\right] \quad (1)$$

Where R_i, G_i, B_i are the mean intensity values of the red, green, and blue color channels of the region, ∇_i is the gradient value obtained by applying the Sobel filter to the grayscale image, and $\mathbb{I}(v_i \in ROI)$ is an indicator function returning 1 if the node is in the tumor region and 0 otherwise.

To make our descriptions richer, especially with regard to complicated patterns, we expand our basic feature vector by incorporating statistical texture features based on grayscale intensity levels. These include the normalized mean μ_i, standard deviation σ_i, skewness γ_i, and kurtosis κ_i, forming a texture vector

$$h_i = \left[\frac{\mu_i}{255}, \frac{\sigma_i}{255}, \gamma_i, \kappa_i\right] \quad (2)$$

The resulting advanced feature vector is obtained by combining the two, formulated as

$$x_i^{adv} = [x_i, h_i] \quad (3)$$

In this way, we ensure that the model can utilize both appearance and texture characteristics for better region description.

3.2.3 Edge Weight Calculation

To improve the ability of Relational Models in Graph Attention Networks (GATs), we use edge weights, which capture the degree of similarity between adjacent nodes. These are computed using the concept of cosine similarity between their feature vectors. The weight for an edge between two nodes v_i and v_j whose feature vectors are x_i and x_j respectively is

$$w_{ij} = \frac{x_i \cdot x_j}{\|x_i\|\|x_j\| + \epsilon} \quad (4)$$

where $x_i \cdot x_j$ represents the dot product of the vectors and $\|x_i\|$ and $\|x_j\|$ represent their L2 norm respectively, while ϵ represents a tiny constant $(1e-8)$. This way, the GAT model will focus more on edges that connect similar nodes in terms of visual and spatial properties through this edge-weighting scheme that depends on node similarity.

3.3 Network Architectures

3.3.1 Graph Convolutional Network (GCN)

The current research uses an architecture consisting of three GCN layers, followed by global pooling and a fully connected layer. The three GCN layers

adjust the features of each node based on its graph structure using the following propagation formula:

$$H^{(l+1)} = \sigma\left(\tilde{D}^{-\frac{1}{2}}\tilde{A}\tilde{D}^{-\frac{1}{2}}H^{(l)}W^{(l)}\right) \quad (5)$$

$H^{(l)}$ is the node feature matrix at layer l; $\tilde{A} = A + I$ is the adjacency matrix that includes self-loops; $\tilde{D}$ is the degree matrix associated with the adjacency matrix $\tilde{A}$; $W^{(l)}$ is the weight matrix at each particular layer; and σ is the ReLU activation function. This updating procedure for the node v_i can be stated as:

$$h_i^{(l+1)} - \sigma\left(\sum_{j\subset\mathcal{N}(i)\cup\{i\}} \frac{1}{\sqrt{\tilde{d}_i\tilde{d}_j}} W^{(l)}h_j^{(l)}\right) \quad (6)$$

Here, $\mathcal{N}(i)$ refers to the set of neighbors of node i, while $\tilde{d}_i$denotes the degree of node i in the graph. Global average pooling is used for all nodes in the graph after applying the last GCN layer to obtain a graph embedding:

$$h_G = \frac{1}{|V|}\sum_{i\in V} h_i^{(L)} \quad (7)$$

where L is the last layer of the GCN network. The resulting vector h_G is then passed to the feedforward layer, which employs the softmax function to determine the output classes:

$$p = softmax(W^{fc}h_G + b^{fc}) \quad (8)$$

with W^{fc} and b^{fc} representing the weights and biases of the classification layer.

3.3.2 Graph Attention Network (GAT)

The Graph Attention Network (GAT) architecture enhances the conventional Graph Convolutional Network (GCN) by integrating attention processes that allow the model to discern the relative significance of adjacent nodes during feature aggregation. For a node v_i , the unnormalized attention coefficient with a neighboring node v_j is computed as:

$$e_{ij} = LeakyReLU\left(a^T\left[Wh_i||Wh_j\right]\right) \quad (9)$$

where W represents a shared learnable weight matrix, a signifies a trainable attention vector, $||$ indicates vector concatenation, and LeakyReLU is the activation function characterized by a negative slope of 0.2. The coefficients are then normalized across the neighbors of node i using the softmax function to obtain attention weights:

$$\alpha_{ij} - \frac{exp(e_{ij})}{\sum_{k\in\mathcal{N}(i)} exp(e_{ik})} \quad (10)$$

ensuring that the importance weights form a valid probability distribution. The updated representation of node v_i is computed is a weighted aggregation of the changed attributes of its neighbors:

$$h_i' = \sigma\left(\sum_{j\in\mathcal{N}(i)} \alpha_{ij}Wh_j\right) \quad (11)$$

where σ is a non-linear activation function, commonly the ReLU. Multi-head attention is utilized to enhance model expressiveness and training stability. In this context, K independent attention mechanisms operate concurrently,with their outputs either concatenated or averaged. When concatenation is used, the final node embedding becomes:

$$h_i' = ||_{k=1}^{K}\sigma\left(\sum_{j\in\mathcal{N}(i)} \alpha_{ij}^k W^k h_j\right) \quad (12)$$

where α_{ij}^k and W^k represent the attention weights and transformation matrix for the $k-th$ head, respectively. In our implementation, we utilize eight attention heads in both of the initial two GAT layers and a single attention head in the final layer. Following the attention layers, a global mean pooling operation is applied to obtain a graph-level embedding, which is then passed through a fully connected layer to perform classification, following the same pipeline used in the GCN architecture.

3.4 Spectral Graph Analysis

3.4.1 Laplacian Matrix and Eigenvalues

To ascertain the structural characteristics of each graph G obtained from an MRI picture, we calculate the normalized graph Laplacian matrix, defined as:

$$L_{norm} = D^{-\frac{1}{2}}LD^{-\frac{1}{2}} = I - D^{-\frac{1}{2}}AD^{-\frac{1}{2}} \quad (13)$$

Here, $L = D - A$ represents the unnormalized Laplacian matrix, where D denotes the degree matrix (a diagonal matrix with D_{ii} corresponding to the degree of node i), A signifies the adjacency matrix of the graph, and I is the identity matrix. This normalization addresses the heterogeneity among nodes ana produces a more stable spectral representation. The eigenvalues $\lambda_1 \leq \lambda_2 \leq \cdots \leq \lambda_n$of L_{norm} are then

computed to extract several spectral characteristics of the graph. These include:

1. **Algebraic Connectivity**(λ_2): The next lowest eigenvalue that gives an understanding of the level of connectivity of the graph. Its high value implies a highly connected network.
2. **Spectral Gap**$(\lambda_2 - \lambda_1)$: It is a measure of how separate are the different components of the graph.
3. **Graph Energy**:

$$E(G) - \sum_{i=1}^{n} |\lambda_i| \quad (14)$$

which quantifies the total spectral complexity of the graph and is often associated with structural richness. These spectral properties are analyzed across graphs corresponding to different tumor types, with the goal of identifying structural patterns or discriminative characteristics that may aid in tumor classification or subtype differentiation.

3.4.2 Statistical Analysis of Spectral Properties

In order to determine whether there is any significant difference in spectral characteristics in relation to the type of tumor, a one-way ANOVA test will be used for each spectral characteristic. The one-way ANOVA test is performed by examining the ratio of between-groups variation to within-groups variation, which is expressed as:

$$F = \frac{MS_{between}}{MS_{within}} \quad (15)$$

whereas $MS_{between}$ indicates the mean square variability between the groups (tumors types), MS_{within} within refers to the mean square variability within the groups. The null hypothesis (H_0) suggests that there is no difference between the means of the spectral properties of the tumors.
The F-statistic is calculated for each of the spectral properties, namely, algebraic connectivity, spectral gap, and graph energy, with its corresponding p-value being employed for testing its statistical significance. If the p-value is found to be lower than 0.05, it implies that the spectral feature has some discriminating power for tumor diagnosis.

3.5 Implementation Details

3.5.1 Graph Construction Algorithm

The following algorithm 1 details the graph construction process:

Algorithm 1: Graph Construction from MRI Image

Input: MRI Image I, Grid Size g, Bounding box bbox (optional)
Output: Graph $G = (V, E, X)$ with node features X

1. Initialize empty node set V, edge set E, and features set X
2. Divide the image I into $g \times g$ grid cells
3. For each cell (i, j):
   a. Extract cell region R_{ij} from image I
   b. Compute mean RGB values R_{ij}, G_{ij}, B_{ij}
   c. Compute gradient magnitude ∇_{ij} using Sobel operators
   d. Set $\text{in\_bbox} = 1$ if cell center is within bbox, otherwise 0
   e. Compute texture features (mean, std, skewness, kurtosis)
   f. Create feature vector $x_i = \left[\frac{R_i}{255}, \frac{G_i}{255}, \frac{B_i}{255}, \frac{\nabla_i}{255}, \text{in\_bbox}\right]$
   g. Add node v_{ij} to V with features x_{ij} to X
4. For each node v_{ij}:
   a. For each of the 8 neighboring cells $(i \pm 1, j \pm 1)$:
   i. If neighbor exists, add edge $(v_{ij}, v_{neighbor})$ to E
   ii. Compute edge weight using cosine similarity between feature vectors
5. Return $G = (V, E, X)$

3.5.2 Model Architecture Details

Figure 2 shows the architecture for both GCN and GAT with the same input layer, followed by global average pooling and a 3-way softmax output. The GCN model consists of graph convolutions using ReLU activation and dropout, followed by a fully connected layer, whereas the GAT model utilizes multi-head attention with ELU activation and two fully connected layers.

Journal of Theoretical and Applied Information Technology
15st September 2026. Vol.104. No.17

ISSN: 1992-8645 www.jatit.org E-ISSN: 1817-3195

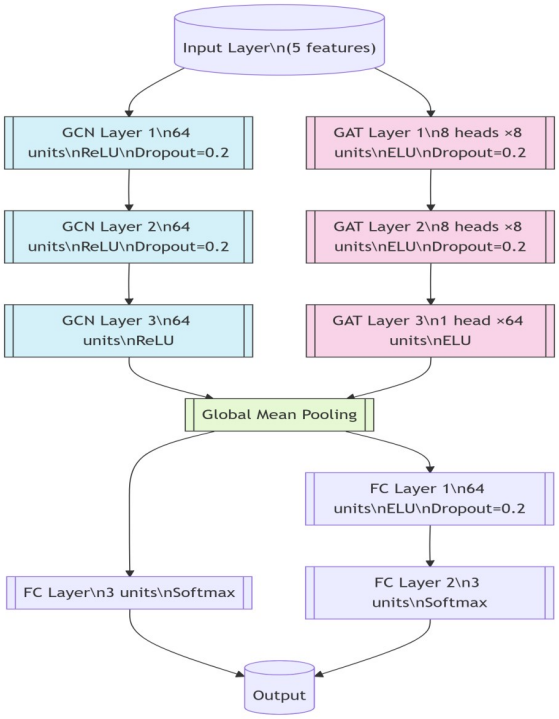

Figure 2 : Unified flowchart comparing the architectures of Graph Convolutional Network (GCN) and Graph Attention Network (GAT).

3.5.3 Model Training

The entire modeling process were executed with the PyTorch and PyTorch Geometric frameworks, leveraging their capabilities for efficient graph-based deep learning. The training process utilized the Adam optimizer with the following hyperparameter settings: a learning rate of 0.001, a batch size of 32, 15 training epochs, a weight decay of $1e-5$, and a dropout rate of 0.2 to mitigate overfitting.The training goal was to reduce the categorical cross-entropy loss, which is defined as:

$$\mathcal{L} = -\frac{1}{N}\sum_{i=1}^{N}\sum_{c=1}^{C} y_{i,c}\log(p_{i,c}) \quad (16)$$

where N represents the quantity of training samples, C signifies the number of target classes (three in this instance), $y_{i,c}$ is a binary indicator that equals 1 if sample i is classified in class c, and $p_{i,c}$ is the model's predicted probability for class c.

The training was performed on a workstation including an Intel Core i7 processor and 16 GB of RAM.To ensure training efficiency and prevent memory leaks in a CPU-constrained environment, memory monitoring and garbage collection routines were explicitly invoked at the end of each epoch.

3.5.4 Traditional Machine Learning Baselines

For comparison, we implemented three traditional machine learning methods:

A. Random Forest: A collection of 100 decision trees use Gini impurity as the condition for splitting .

B. Support Vector Machine (SVM): Using the Radial Basis Function (RBF) kernel with $C = 1.0$ and $\text{gamma} = 'scale'$.

C. Gradient Boosting: Using 100 estimators with a maximum depth of 3 and a learning rate of 0.1.

Table 1 shows the feature extraction methods applied, which include HOG, LBP, and statistical features, together with their main parameters. The table gives a good comparison between the feature extraction settings.

Table 1 : *Summary of feature extraction methods and their parameters.*

Feature Type	Parameters
Histogram of Oriented Gradients (HOG) features	- Orientations: 9 - Pixels per cell: (8, 8) - Cells per block: (2, 2)
Local Binary Pattern (LBP) features	-Radius: 3 - Number of points: 24 - Method: uniform
Basic statistical features	- Mean intensity - Standard deviation of intensity

The feature vectors were concatenated to form a comprehensive representation of the MRI images.

3.5.5 Evaluation Metrics

All models' performance was assessed utilizing the subsequent metrics:

1. **Accuracy:** The ratio of accurately categorized samples.

$$\text{Accuracy} = \frac{\text{Number of correctly classified samples}}{\text{Total number of samples}} \quad (17)$$

2. **Precision**: The ratio of true positive predictions to the total positive forecasts for each class.

$$Precision_c = \frac{TP_c}{TP_c + FP_c} \quad (18)$$

Journal of Theoretical and Applied Information Technology
15st September 2026. Vol.104. No.17

ISSN: 1992-8645 www.jatit.org E-ISSN: 1817-3195

3. **Recall**: The ratio of true positive forecasts to the total number of real positives for each class.

$$Recall_c = \frac{TP_c}{TP_c + FN_c} \quad (19)$$

4. **F1-Score:** The harmonic mean of precision and recall for each class.

$$F1 - Score_c = 2 \times \frac{Precision_c \times Recall_c}{Precision_c + Recall_c} \quad (20)$$

Where TP_c is the number of true positives for class, FP_c is the number of false positives for class and FN_c is the number of false negatives for class

5. **Statistical Significance**: To determine if the performance difference between models is statistically significant, we conducted a t-test on the accuracy of predictions for each sample

4. RESULTS

4.1 Model Performance Comparison

4.1.1 Classification Accuracy

Table 2 shows the performance accuracy of different models for the validation dataset. The maximum accuracy is seen for GAT, at 77.37%. The second-best is Random Forest, followed by GCN, Gradient Boosting, and SVM, at 76.67%, 71.53%, 72.22

Table 2: Accuracy of classification by different models on the validation data set.

Model	Accuracy (%)
GAT (Novel Graph)	77.37
GCN (Graph)	71.53
Random Forest (Traditional)	76.67
Gradient Boosting (Traditional)	72.22
SVM (Traditional)	62.22

The results show the effectiveness of the proposed GAT architecture, which is superior to both the GCN model and classical machine learning methods.

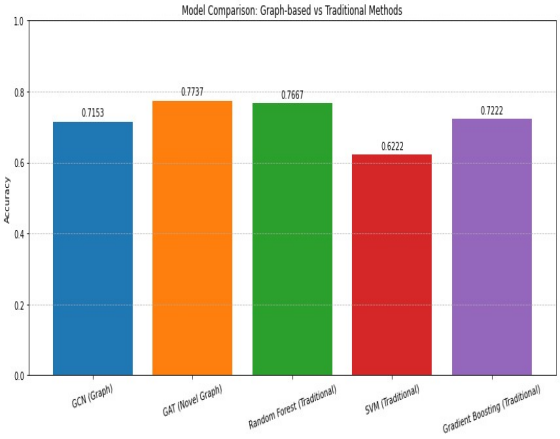

Figure 3: Model Comparison: Graph-based vs Traditional Methods

4.1.2 Detailed Classification Metrics

Table 3 delineates the precision, recall, and F1-score for each model across the three tumor classifications.

Table 3: Precision, recall, and F1-score for each model and tumor type.

Model	Tumor Type	Precision	Recall	F1-Score	Support
GAT	Glioma	0.70	0.73	0.71	135
	Meningioma	0.76	0.71	0.73	140
	Pituitary	0.86	0.88	0.87	136
	Average	0.77	0.77	0.77	411
GCN	Glioma	0.70	0.56	0.63	135
	Meningioma	0.65	0.71	0.68	140
	Pituitary	0.79	0.87	0.83	136
	Average	0.71	0.72	0.71	411
Random Forest	Glioma	0.83	0.63	0.72	30
	Meningioma	0.71	0.80	0.75	30
	Pituitary	0.79	0.87	0.83	30
	Average	0.77	0.77	0.76	90
SVM	Glioma	0.53	0.63	0.58	30
	Meningioma	0.70	0.63	0.67	30
	Pituitary	0.67	0.60	0.63	30
	Average	0.63	0.62	0.62	90
Gradient Boosting	Glioma	0.61	0.63	0.62	30
	Meningioma	0.65	0.67	0.66	30
	Pituitary	0.93	0.87	0.90	30
	Average	0.73	0.72	0.73	90

The GAT model shows consistent performance across all tumor types, with particularly high precision and recall for the pituitary tumor class. The GCN model performs well on pituitary tumors but struggles with glioma classification. Traditional methods show varied performance, with Random Forest achieving comparable results to the GAT model, particularly for glioma and pituitary tumors.

4.1.3 Confusion Matrices

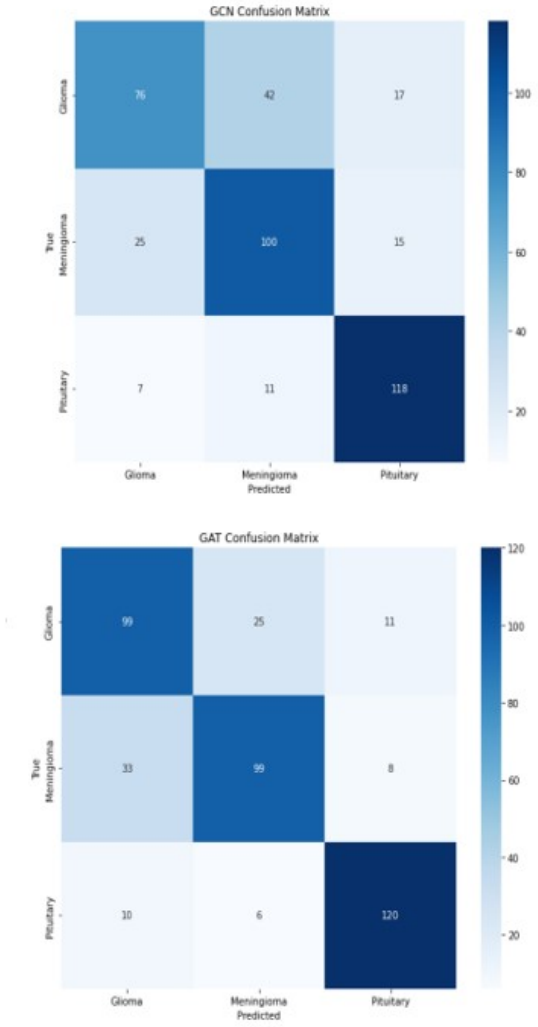

Figure 4 :The confusion matrices for the GCN and GAT models on the validation dataset.

It is clear from the confusion matrices that the GCN model is not very efficient in classifying glioma tumors, having a recall score of only 56%, but for meningiomas and pituitary tumors, the values are 71% and 87%, respectively. On the other hand, when compared with the GCN model, the GAT model has higher values in classifying gliomas (with 73% recall), while retaining good performance in meningiomas and pituitary tumors.

4.1.4 Statistical Significance

To ascertain the statistical significance of the performance disparity between the GCN and GAT models, we conducted a t-test on the individual accurate and incorrect predictions. The t-statistic was 1.9214, accompanied by a p-value of 0.0550, which slightly exceeds the traditional significance threshold of 0.05.

This result suggests that while the GAT model outperforms the GCN model, the improvement is just short of being statistically significant at the 95% confidence level. However, the p-value is close enough to 0.05 to warrant consideration of the GAT model's practical advantages, especially given its improved interpretability through attention mechanisms.

4.2 Training Dynamics

4.2.1 Learning Curves

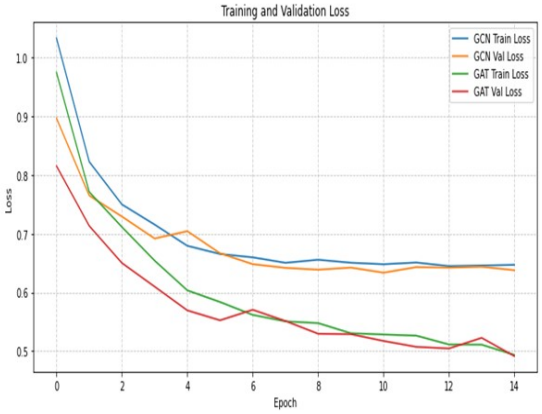

Figure 5: Demonstrates the training and validation loss trajectories for both the GCN and GAT models throughout 15 epochs.

From the graphs, it is evident that the GCN model experiences quick convergence during the early stages, with the training loss and validation loss decreasing to 0.6469 and 0.6377, respectively, after 15 epochs. On the other hand, the GAT model shows a faster rate of convergence, with its training loss and validation loss decreasing to 0.4935 and 0.4914, respectively.

Table 4 presents the epoch-by-epoch training results for the GCN model, showing the progression of training and validation loss and accuracy.

Table 4: Epoch-by-epoch training results for the GCN model

Epoch	Train Loss	Train Acc	Val Loss	Val Acc	Time (s)	Memory (MB)
1	1.0326	0.4794	0.8964	0.6034	236.07	475.3
2	0.8225	0.6093	0.7648	0.6107	236.34	475.4
3	0.7497	0.6453	0.7291	0.6521	237.56	475.6
4	0.7154	0.6796	0.6917	0.7105	236.70	475.7
5	0.6793	0.7104	0.7042	0.7032	236.17	475.7
6	0.6653	0.7086	0.6665	0.7056	236.55	475.5
7	0.6596	0.7163	0.6480	0.7129	236.19	475.7
8	0.6503	0.7231	0.6417	0.6934	236.63	476.0
9	0.6555	0.7253	0.6386	0.7105	237.20	476.0
10	0.6504	0.7268	0.6422	0.6788	237.84	475.8
11	0.6479	0.7245	0.6335	0.7080	618.03	471.5
12	0.6508	0.7226	0.6430	0.7056	736.64	471.5
13	0.6447	0.7253	0.6421	0.7080	717.74	456.0
14	0.6457	0.7208	0.6436	0.7032	233.67	456.1
15	0.6469	0.7245	0.6377	0.7153	282.48	456.3

Table 5: Epoch-by-epoch training results for the GAT model

Epoch	Train Loss	Train Acc	Val Loss	Val Acc	Time (s)	Memory (MB)
1	0.9741	0.4948	0.8151	0.5912	354.98	562.3
2	0.7709	0.6428	0.7132	0.6983	262.50	545.9
3	0.7113	0.6962	0.6500	0.7153	263.34	547.2
4	0.6540	0.7258	0.6098	0.7202	293.75	548.4
5	0.6034	0.7489	0.5693	0.7153	542.53	545.1
6	0.5836	0.7546	0.5524	0.7445	1204.85	544.4
7	0.5616	0.7598	0.5703	0.7348	995.59	542.6
8	0.5506	0.7675	0.5512	0.7543	1379.88	541.4
9	0.5476	0.7628	0.5295	0.7494	748.76	541.8
10	0.5304	0.7690	0.5288	0.7616	618.37	543.9
11	0.5283	0.7822	0.5172	0.7640	416.93	545.3
12	0.5263	0.7809	0.5072	0.7689	259.31	545.5
13	0.5113	0.7884	0.5045	0.7713	624.26	542.5
14	0.5110	0.7839	0.5225	0.7786	285.96	545.6
15	0.4935	0.7943	0.4914	0.7737	278.15	545.6

Journal of Theoretical and Applied Information Technology
15st September 2026. Vol.104. No.17

ISSN: 1992-8645 www.jatit.org E-ISSN: 1817-3195

4.2.2 Accuracy Progression

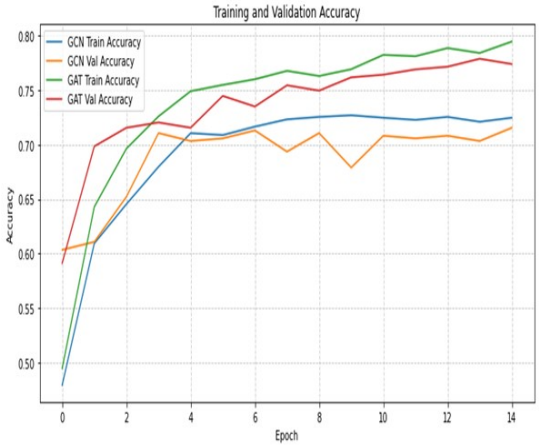

Figure 6: Over the 15 epochs, both models' training and validation accuracy curves show

Over the 15 seasons, the training accuracy of the GCN model rises from 47.94% to 72.45%; its validation accuracy rises from 60.34% to 71.53%. The validation accuracy plateaus about epoch 7, suggesting little more learning.

By contrast, the GAT model's training accuracy rises from 49.48% to 79.43% and its validation accuracy rises from 59.12% to 77.37%. With a consistent rise in validation accuracy even in the last epochs, the GAT model keeps becoming better during the training process. These accuracy curves especially help to confirm the efficiency of the GAT architecture, especially in terms of its capacity to keep learning relevant patterns all during the training process.

4.2.3 Memory Usage

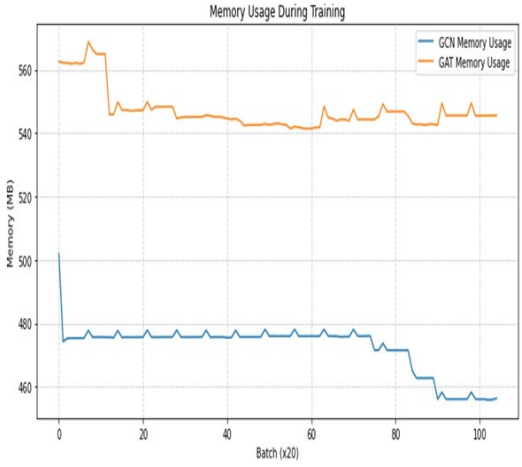

Figure 7 : The memory usage of both models during training.

The GCN model maintains a relatively constant memory usage of around 475 MB throughout the training process, with a slight decrease to 456 MB in the later epochs.
The GAT model shows a higher memory usage of around 545 MB, which is expected given its more complex architecture with attention mechanisms. The memory usage remains stable throughout training, with minor fluctuations between 541 MB and 562 MB.
Although the GAT model uses up more memory, it is not an insurmountable problem, especially given the better results it offers.

4.3 Graph Properties Analysis

4.3.1 Node Importance Patterns

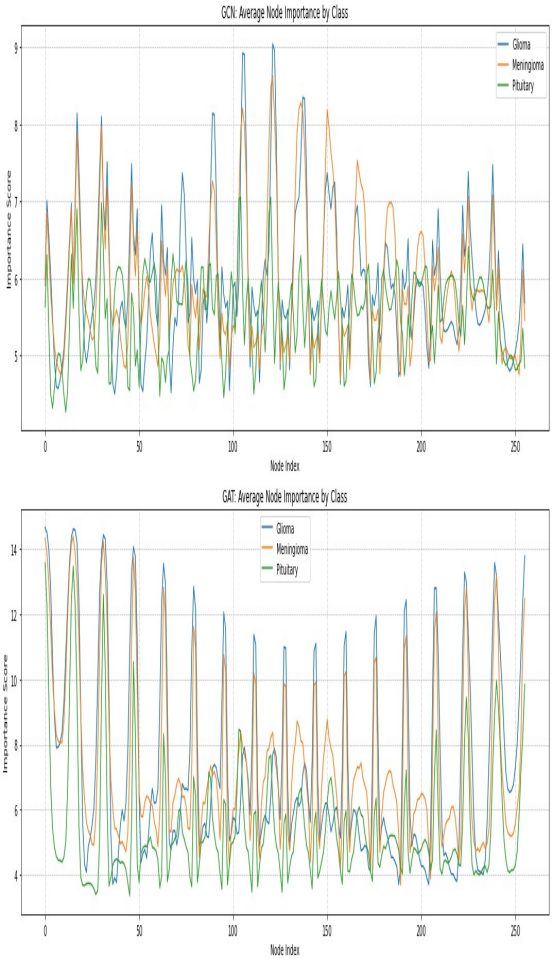

Figure 8: Provides an illustration of the general trend in the average importance of nodes in the GCN and GAT architectures under different tumor types.

For the GCN model, the node importance plots vary depending on the type of tumor considered. In the case of the glioma tumor, the plot is centered at the

center while for the meningioma tumor, the plot is distributed evenly throughout, and finally, the pituitary tumor is concentrated in certain regions. The GAT network has better-defined plots in terms of the importance of the nodes in each tumor type.

4.3.2 Spectral Graph Properties

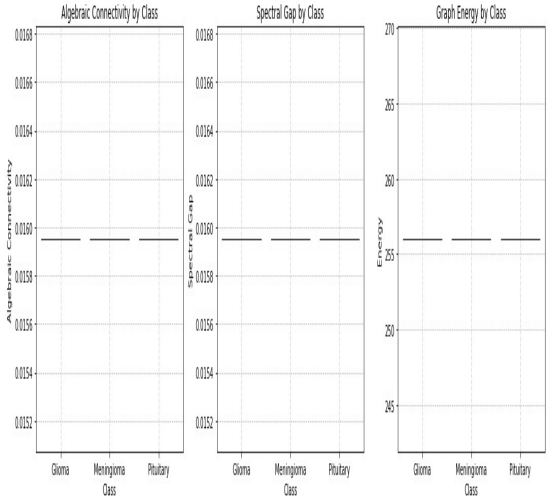

Figure 9: Box plots of different graph spectrum characteristics per tumor type are presented here.

The algebraic connectivity (λ_2) exhibits significant variance across different tumor types, where pituitary tumors have greater algebraic connectivity than gliomas and meningiomas, implying that graphs associated with pituitary tumors have relatively greater connectivity.

The spectral gap $(\lambda_2 - \lambda_1)$ is consistent with the above trend, which suggests that graphs associated with pituitary tumors have a large spectral gap and thus a stronger connection structure.

However, the ANOVA test for these spectral properties produced non-significant p-values ($p > 0.05$), signifying that while there are observable differences in spectral properties between tumor types, these differences are not statistically significant in our dataset.

4.4 Visualizations

4.4.1 Attention Mechanism Visualization

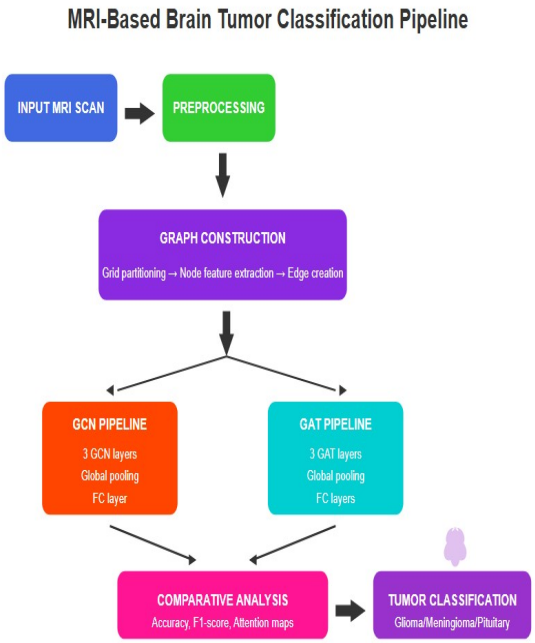

Figure 10 : Visualizations of the attention mechanisms for both GCN and GAT models on sample images from each tumor type.

In terms of glioma, the GCN model attends to the general location of the tumor, whereas the GAT model attends to the tumor edge and structure. With regard to meningioma cases, the GCN model shows a scattered pattern of attention, but the GAT model concentrates on the characteristic edges and structures. Concerning pituitary tumors, both models attend to the tumor site; however, the GAT model provides a clear focus on the tumor structure and anatomy surrounding it.

4.4.2 Graph Representation Visualization

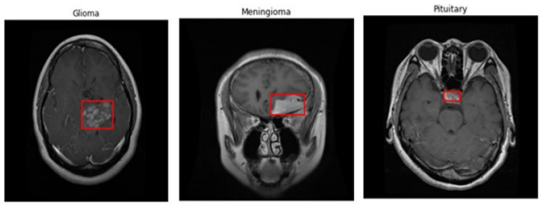

Figure 11: Illustrates the nodes (image areas) and edges (relationships between regions) with node colors indicating feature values and edge weights seen through line thickness, so illustrating the graph representation of sample MRI images.

The graph models incorporate the intricate spatial correlations within the MRI scans, with increased edges around the tumors and within the tumors. The large edge weights found in areas that look similar help detect correlation, allowing for an effective

consideration of local features and correlations as opposed to traditional models using pixels.

5. DISCUSSION

5.1 Interpretation of Results

The effectiveness of graph-based techniques, specifically Graph Attention Network (GAT), is clearly evident from the experiment results pertaining to the classification of brain tumors using MRI images. With Random Forest the best performer among them at 76.67% accuracy, the GAT model obtained an accuracy of 77.37%, surpassing both the Graph Convolutional Network (GCN) with 71.53% accuracy and conventional machine learning techniques.Many elements help the GAT model to show better performance:

1.**Attention Mechanism**: The GAT can concentrate on the most pertinent areas for classification by assigning different value to various nearby nodes. In brain tumor classification, where some areas e.g., tumor boundaries, particular internal structures are more diagnostically informative than others, this is especially important.

2. **Edge Weighting**: Edge weights based on feature similarity give the GAT model extra structural information and helps it to better capture the links between image areas.

3. **Advanced Feature Extraction**: The model can capture more intricate patterns in the MRI scans by including Haralick texture elements next to fundamental color and gradient elements.

Based on the confusion matrix results, all the models showed the best performance for pituitary tumors owing to their unique characteristics. Specifically, the proposed GAT model showed balanced classification accuracy for all tumor types as well as better identification of gliomas than the GCN model. Results from training indicate that GAT models exhibited steady training performance throughout the training period.

From the results obtained from attention visualization, the GAT model exhibited interest in regions such as the boundaries of the tumor as well as structures of the tumor. Conversely, the spectral graph analysis provided useful insights about the tumor structures.

5.2 Advantages of Graph-based Approaches

The graph representation of brain tumors for image classification is an adaptive way that represents MRI images efficiently by accounting for structural inconsistencies and relationships. The use of such a method can increase classification performance by employing relational reasoning and making the model explainable using attention. Moreover, the graph framework makes it easy to incorporate other clinical features.

5.3 Clinical Implications

The increased accuracy and interpretability of the GAT algorithm imply many implications for the clinic. The GAT algorithm will help the radiologists by providing automatic classification of the tumor and its visualization through attention maps of the suspicious areas of the tumor. This approach will not only increase the accuracy of detection but also avoid any discrepancies between observers. Automatic pre-processing of MRI images is expected to increase the speed and quality of the diagnostic process. At the same time, the analysis provided via attention maps will give some important information about the detected tumors.

5.4 Limitations

Although there are positive results, some of the drawbacks in the study should be mentioned. Firstly, even though the used database is rather large, an even greater amount of data with a variety of characteristics would allow for better generalization. Secondly, only T1-weighted contrast-enhanced MRI scans have been utilized for the analysis; additional sequences, like T2 and FLAIR, could be useful. Moreover, the addition of the binary variable indicating the presence of a tumor is also rather rudimentary because it cannot properly reflect the nature of tumor invasion. In addition, the use of just three brain tumor classes by the algorithm makes it less valuable for practical purposes; improving this will make it much more useful for further classification of other tumors. Lastly, although the GAT model is very efficient, its high computational complexity limits its immediate application.

6. CONCLUSION AND FUTURE WORK

6.1 Overview of Contributions

In this work, we have presented a new graph-based approach to classify brain tumors based on MRI images. There are several aspects to our contributions. Firstly, we created a graph structure which is capable of representing both image region characteristics and relations between them, allowing us to perform a more context-sensitive analysis. Secondly, we have designed a new graph

attention model which uses edge information and is optimized for solving the problem of brain tumor classification. Thirdly, we have performed an extensive comparison of different graph-based methods, including GCN and GAT, with classical machine learning techniques like Random Forest, SVM, and Gradient Boosting, and discussed the benefits of graph models. Moreover, we have conducted research into the spectral characteristics of our graphs and compared them for different types of tumors, examining their connection to the quality of classification. Moreover, visualization was employed in order to examine how the attention mechanisms work in the GAT architecture, offering clinically meaningful information about the most significant regions when identifying the tumors.

As shown by the results of the experiments conducted, the proposed GAT architecture is highly efficient, achieving 77.37% accuracy, surpassing not only the GCN architecture but also other traditional machine learning models.

6.2 Future Directions

Future directions for this research could be combining multimodal MR images with hierarchical graphs to improve classification performance. Integration of both tumor segmentation and classification in a single MTL framework along with longitudinal studies can prove useful in making the use of such methods in clinical settings more common. Other possible directions could be improving model explainability, transferring learning from one patient to another, and validating models on clinical data. Research with spectral graphs constructed using larger amounts of data can prove useful in better understanding of brain tumors.

Overall, the suggested Graph Attention Network model shows that the application of graph learning methods in brain tumor classification leads to effective results.

REFERENCES:

[1] Louis, D. N., Perry, A., Reifenberger, G., Von Deimling, A., Figarella-Branger, D., Cavenee, W. K., . & Ellison, D. W. (2016). The 2016 World Health Organization classification of tumors of the central nervous system: a summary. *Acta neuropathologica*, 131(6), 803-820.

[2] Bauer, S., Wiest, R., Nolte, L. P., & Reyes, M. (2013). A survey of MRI-based medical image analysis for brain tumor studies. *Physics in Medicine & Biology*, 58(13), R97.

[3] Dhermain, F. G., Hau, P., Lanfermann, H., Jacobs, A. H., & van den Bent, M. J. (2010). Advanced MRI and PET imaging for assessment of treatment response in patients with gliomas. *The Lancet Neurology*, 9(9), 906-920.

[4] Litjens, G., Kooi, T., Bejnordi, B. E., Setio, A. A. A., Ciompi, F., Ghafoorian, M., . & Sánchez, C. I. (2017). A survey on deep learning in medical image analysis. *Medical image analysis*, 42, 60-88.

[5] Akkus, Z., Galimzianova, A., Hoogi, A., Rubin, D. L., & Erickson, B. J. (2017). Deep learning for brain MRI segmentation: state of the art and future directions. *Journal of digital imaging*, 30(4), 449-459.

[6] Abrol, S., Kotrotsou, A., Salem, A., Zinn, P. O., & Colen, R. R. (2017). Radiomic phenotyping in brain cancer to unravel hidden information in medical images. *Topics in Magnetic Resonance Imaging*, 26(1), 43-53.

[7] Sheller, M. J., Edwards, B., Reina, G. A., Martin, J., Pati, S., Kotrotsou, A., . & Bakas, S. (2020). Federated learning in medicine: facilitating multi-institutional collaborations without sharing patient data. *Scientific reports*, 10(1), 1-12.

[8] Sudre, C. H., Li, W., Vercauteren, T., Ourselin, S., & Cardoso, M. J. (2017). Generalised dice overlap as a deep learning loss function for highly unbalanced segmentations. *In Deep learning in medical image analysis and multimodal learning for clinical decision support* (pp. 240-248). Springer.

[9] Menze, B. H., Jakab, A., Bauer, S., Kalpathy-Cramer, J., Farahani, K., Kirby, J., . & Van Leemput, K. (2015). The multimodal brain tumor image segmentation benchmark (BRATS). *IEEE transactions on medical imaging*, 34(10), 1993-2024.

[10] Maier, O., Wilms, M., & Handels, H. (2016). *Image features for brain lesion segmentation using random forests*. In Brainlesion: glioma, multiple sclerosis, stroke and traumatic brain injuries (pp. 119 130). Springer.

[11] Wu, Z., Pan, S., Chen, F., Long, G., Zhang, C., & Philip, S. Y. (2020). A comprehensive survey on graph neural networks. *IEEE transactions on neural networks and learning systems*, 32(1), 4-24.

[12] Gilmer, J., Schoenholz, S. S., Riley, P. F., Vinyals, O., & Dahl, G. E. (2017). Neural message passing for quantum chemistry. *In International conference on machine learning* (pp. 1263-1272). PMLR.

[13] Kipf, T. N., & Welling, M. (2016). *Semi-supervised classification with graph convolutional networks.* arXiv preprint arXiv:1609.02907.

[14] Parisot, S., Ktena, S. I., Ferrante, E., Lee, M., Guerrero, R., Glocker, B., & Rueckert, D. (2018). Disease prediction using graph convolutional networks: application to autism spectrum disorder and Alzheimer's disease. *Medical image analysis*, 48, 117-130.

[15] Kipf, T. N., & Welling, M. (2017). Semi-supervised classification with graph convolutional networks. In *International Conference on Learning Representations* (ICLR).

[16] Veličković, P., Cucurull, G., Casanova, A., Romero, A., Liò, P., & Bengio, Y. (2018). Graph attention networks. In *International Conference on Learning Representations* (ICLR).

[17] Zacharaki, E. I., Wang, S., Chawla, S., Soo Yoo, D., Wolf, R., Melhem, E. R., & Davatzikos, C. (2009). Classification of brain tumor type and grade using MRI texture and shape in a machine learning scheme. *Magnetic Resonance in Medicine*, 62(6), 1609-1618.

[18] Kharrat, A., Gasmi, K., Messaoud, M. B., Benamrane, N., & Abid, M. (2010). A hybrid approach for automatic classification of brain MRI using genetic algorithm and support vector machine. *Leonardo journal of sciences*, 17(1), 71-82.

[19] Zacharaki, E. I., Kanas, V. G., & Davatzikos, C. (2011). Investigating machine learning techniques for MRI-based classification of brain neoplasms. *International journal of computer assisted radiology and surgery*, 6(6), 821-828.

[20] El-Dahshan, E. S. A., Hosny, T., & Salem, A. B. M. (2010). Hybrid intelligent techniques for MRI brain images classification. *Digital Signal Processing*, 20(2), 433-441.

[21] Afshar, P., Mohammadi, A., & Plataniotis, K. N. (2018). Brain tumor type classification via capsule networks. In 2018 25th *IEEE International Conference on Image Processing* (ICIP) (pp. 3129-3133). IEEE.

[22] Swati, Z. N. K., Zhao, Q., Kabir, M., Ali, F., Ali, Z., Ahmed, S., & Lu, J. (2019). Brain tumor classification for MR images using transfer learning and fine-tuning. *Computerized Medical Imaging and Graphics,* 75, 34-46.

[23] Sajjad, M., Khan, S., Muhammad, K., Wu, W., Ullah, A., & Baik, S. W. (2019). Multi-grade brain tumor classification using deep CNN with extensive data augmentation. *Journal of computational science*, 30, 174-182.

[24] Havaei, M., Davy, A., Warde-Farley, D., Biard, A., Courville, A., Bengio, Y., . & Larochelle, H. (2017). Brain tumor segmentation with deep neural networks. *Medical image analysis*, 35, 18-31.

[25] Li, C., Gore, J. C., & Davatzikos, C. (2014). Multiplicative intrinsic component optimization (MICO) for MRI bias field estimation and tissue segmentation. *Magnetic resonance imaging*, 32(7), 913-923.

[26] Parisot, S., Ktena, S. I., Ferrante, E., Lee, M., Moreno, R. G., Glocker, B., & Rueckert, D. (2017). Spectral graph convolutions for population-based disease prediction. In *International Conference on Medical Image Computing and Computer-Assisted Intervention* (pp. 177-185). Springer.

[27] Kazi, A., Krishna, S. A., Shekarforoush, S., Kortuem, K., Albarqouni, S., & Navab, N. (2019). Graph convolution based attention model for personalized disease prediction. In *International Conference on Medical Image Computing and Computer-Assisted Intervention* (pp. 122-130). Springer.

[28] Zhang, J., Hu, H., Chen, S., Huang, Y., & Metaxas, D. N. (2021). Learning dual encoding graph convolutional networks for multi-modal brain tumor segmentation. In *International Conference on Medical Image Computing and Computer-Assisted Intervention* (pp. 600-610). Springer.

[29] Vaswani, A., Shazeer, N., Parmar, N., Uszkoreit, J., Jones, L., Gomez, A. N., . & Polosukhin, I. (2017). Attention is all you need. In *Advances in neural information processing systems* (pp. 5998-6008).

[30] Schlemper, J., Oktay, O., Schaap, M., Heinrich, M., Kainz, B., Glocker, B., & Rueckert, D. (2019). Attention gated networks: Learning to leverage salient regions in medical images. *Medical image analysis*, 53, 197-207.

[31] Oktay, O., Schlemper, J., Folgoc, L. L., Lee, M., Heinrich, M., Misawa, K., . & Glocker, B. (2018). *Attention u-net: Learning where to*

look for the pancreas. arXiv preprint arXiv:1804.03999.

[32] Chung, F. R., & Graham, F. C. (1997). Spectral graph theory. *American Mathematical Society.*

[33] Shi, J., & Malik, J. (2000). Normalized cuts and image segmentation. *IEEE Transactions on pattern analysis and machine intelligence*, 22(8), 888-905.

[34] Von Luxburg, U. (2007). A tutorial on spectral clustering. *Statistics and computing*, 17(4), 395-416.

[35] Belkin, M., & Niyogi, P. (2003). Laplacian eigenmaps for dimensionality reduction and data representation. *Neural computation*, 15(6), 1373-1396.

[36] Zhang, H., & Hancock, E. R. (2008). Graph spectral image smoothing using the heat kernel. *Pattern Recognition*, 41(11), 3328-3342.

[37] Shiee, N., Bazin, P. L., Ozturk, A., Reich, D. S., Calabresi, P. A., & Pham, D. L. (2010). A topology preserving approach to the segmentation of brain images with multiple sclerosis lesions. *NeuroImage*, 49(2), 1524-1535.